Fermi National Accelerator Laboratory

FERMILAB-Pub-80/91-EXP
7180.236

(Submitted to Nucl. Phys. B)

A MEASUREMENT OF THE ENERGY DEPENDENCE OF THE INCLUSIVE YIELD OF HIGH P_t EVENTS TRIGGERED BY A LARGE SOLID ANGLE CALORIMETER

V. Cook, G. Hicks, P. M. Mockett, J. E. Rothberg,
R. W. Williams and K. K. Young
University of Washington, Seattle, Washington 98195

and

P. Limon, P. Mantsch, J. R. Orr, and S. Pruss
Fermi National Accelerator Laboratory, Batavia, Illinois 60510

and

W. P. Oliver
Tufts University, Medford, Massachusetts 02155

November 1980

Operated by Universities Research Association Inc. under contract with the United States Department of Energy

A Measurement of the Energy Dependence of the Inclusive Yield of High P_t Events Triggered by a Large Solid Angle Calorimeter.

V. Cook, G. Hicks[1], P. M. Mockett, J. E. Rothberg,

R. W. Williams and K. K. Young

University of Washington
Seattle, Washington 98195

P. Limon, P. Mantsch, J. R. Orr, and S. Pruss

Fermi National Accelerator Laboratory
P. O. Box 500
Batavia, Illinois 60510

and

W. P. Oliver

Tufts University
530 Boston Avenue
Medford, Massachusetts 02155

ABSTRACT

Large aperture calorimeter measurements of high transverse momentum events from 100, 200, and 340 GeV pp collisions are reported. The cross sections are higher by one to two orders of magnitude than the yield expected from uncorrelated statistical fluctuations in multi-particle events. The exponential slopes in x_t, of the yields exhibited a systematic change with $\sqrt{s}$. ($x_t = 2P_t/\sqrt{s}$). The events are shown to be more diffuse than pure jets as produced in e^+e^- collisions. However, these events are consistent with a QCD-inspired 4-jet model.

1. Now at Bell Laboratories, Crawford-Corner Road, Holmdel, N.J. 07733.

1. Introduction

This paper presents measurements of the properties of high energy p-p collisions in which a group of particles carries off transverse momentum which is an appreciable fraction, typically $x_t \sim 0.3$ to 0.5 of the maximum possible ($x_t = 2P_t/\sqrt{s}$). The experiment was motivated by the possibility that total event measurements may be relatively unbiased reflections of elementary hard-scattering processes [1]. Strong indications of these hard-scattering processes have been observed in single particle high-P_t cross section measurements. It was believed that observation of the jet of particles, rather than a single daughter particle, would greatly reduce the uncertainties in interpretation.

We performed our measurements with a large-aperture (2.3 steradians in the center-of-mass frame) calorimeter. A calorimeter device was chosen so that we would be sensitive to all the hadrons in the jet. A calorimeter has the additional advantage of providing a prompt signal, representing the total P_t, that can be utilized as a trigger for the apparatus. These advantages are well recognized. Two other searches for hadron jets with calorimeters, E260[2] and E395[3], have been undertaken at Fermilab.

We have obtained the yield and profiles of inclusive multiparticle high-P_t events. We have measured the level of P_t contribution from particles far from the central axis of such events. The level of this contribution, and other features of our data, force us to introduce a non-jet component in the analysis. The two components are consistent with a four-jet-model picture. A particular model of this type has been used by E260[2] in their analysis.

2. Experimental Arrangement

2.1 Overall Set-up.

The experiment was set up in the M1 beam line in the Meson Lab at Fermilab. The calorimeter formed one arm of a two-arm experiment. The layout of the experimental apparatus is shown in Fig. 1.

The M1 line provided a beam of protons for momenta up to 340 GeV/c (with cherenkov identification at lower momenta) which impinged on a 30 cm long liquid hydrogen target. An array of scintillation counters (not shown) was placed about 2m upstream of the hydrogen target to veto events that came from upstream of the target. The hydrogen target was positioned as shown in Fig. 1 for beam momenta of 100 and 200 GeV/c. For the highest beam momentum, 340 GeV/c, the target was moved 1.04m upstream to maintain the acceptance of the calorimeter at approximately the same position in the center-of-mass frame near $\Theta^* = 90^\circ$.

Seventeen planes of multiwire proportional chambers were used downstream of the target to measure the outgoing particles.

For calibration purposes, a sweeping magnet with adjustable azimuthal orientation was placed 10m upstream of the hydrogen target. Calibration runs were taken with the beam line tuned to momenta between 10 and 100 GeV/c. The beam electrons were identified by a Cerenkov counter. By varying the orientation and magnetic field in the sweeping magnet, electrons and hadrons of known momentum could be directed at the face of the calorimeter. The response of the calorimeter was found to be uniform and stable over the two years the experiment was in place.

2.2 The Calorimeter.

The calorimeter was composed of two independent sections. The front section was constructed of eight 0.64 cm thick sheets of lead interleaved with 0.64 cm thick sheets of plastic scintillator. The rear section was constructed of 32 2.54 cm thick slabs of stainless steel interleaved with 0.64 cm thick sheets of plastic scintillator. An isometric drawing of the calorimeter is shown in Fig. 2. Each sheet of plastic scintillator was formed by a series of adjacent equal-width strips. The orientation of the strips was alternated between the horizontal and vertical directions at each successive depth in the calorimeter to give both x and y readout. In each section a sum over the longitudinal development of the shower was performed by adding the light from corresponding counters at the various depths. The vertical counters were broadened in depth so that a fixed angular acceptance was maintained. In effect, each section of the calorimeter was divided into horizontal and vertical segments.

The lead section was .52m wide by 1.02m high positioned so that the nearest edge was 15 cm from the beam. The aperture of the steel calorimeter at the mean shower depth was .59 m wide by 1.02 m high and positioned so that the nearest edge was 17 cm from the beam. The calorimeter was oriented so that its inner edge formed an angle of 43 mrad with the beam line.

2.3 Summary of Calorimeter Response.

The reponse of the calorimeter to electrons and hadrons of known momentum was measured in special calibration runs. The fractional resolution of the electron energy measurement in the lead section was measured to be

$\sigma/E = .26/\sqrt{E(GeV)}$. The fractional resolution of the hadron energy measurement in the steel section was measured to be $\sigma/E = .81/\sqrt{E(GeV)}$. The measured energy response as well as measurements of the lateral spreading of the hadron showers in the steel section were incorporated in a Monte Carlo model of the calorimeter. A more detailed account of the calorimeter and its measured response is given elsewhere [4].

Because the lead section was predominantly sensitive to photons, while the steel section was precominantly sensitive to hadrons, the overall calibration constant for each section was set so that the sum would give the correct mean energy for either hadronic or electromagnetic energy, or of course any combination.

2.4 Triggering Scheme.

The gains of the phototubes which viewed the different segments of the calorimeter were set so that each phototube pulse height was approximately proportional to the total P_t carried by all particles which entered that particular segment. The phototubes pulses were added electronically to form a pulse which represented the total P_t of all particles which entered the calorimeter. Two P_t-thresholds (1.5 GeV/c and 3.0 GeV/c) were used and the lower threshold events were prescaled so that only a fraction of these events were recorded.

3. Event Reconstruction.

3.1 Vertex Finding.

The information from the 17 planes of multiwire chambers downstream of

the target was used coherently to locate the vertex of the interaction which produced the calorimeter trigger. The presence of the multiwire planes was essential since the calorimeter provides very little information on its own of the source of the energy it detects.

After the cut on the vertex was made, the target empty yield to target full yield ratio became less than 0.04, which is consistent with residual gas in the flask. Reconstruction of tracks which originated upstream of the target was also performed to eliminate events that originated upstream but which nevertheless produced a vertex due to a secondary interaction within the target.

3.2 Calorimeter Reconstruction.

The calorimeter measured the total energy carried by all entering particles as well as the x and y profiles of the energy distribution pattern. The lead and steel sections provided independent measurements, the lead section measuring the energy and distribution of π^0's and the steel section measuring the energy and distribution of the remaining hadrons.

The four-momentum vector of the group of particles entering each section of the calorimeter was reconstructed by the following procedure:

(1) The transverse momentum components are given by

$$P_x = E\langle x\rangle/R \text{ and } P_y = E\langle y\rangle/R$$

where E is the total energy measured by the section and $\langle x\rangle$ and $\langle y\rangle$ are the mean positions of the energy. Denoting the distance from the vertex to the mean shower depth in the calorimeter section by z, then

$$R = (\langle x\rangle^2 + \langle y\rangle^2 + z^2)^{\frac{1}{2}}$$

The measured energy is related to momentum by assuming the particles are photons (lead section) or pions (iron section). The small angle approximation used is correct to better than 1% for our geometry.

(2) To obtain P_z we calculate the invariant mass of the group of particles from the relation

$$m^2 = E^2(\sigma_x^2 + \sigma_y^2)/R^2 + E^2(\langle x\rangle^2\sigma_x^2 + \langle y\rangle^2\sigma_y^2 + 2\langle x\rangle\langle y\rangle\sigma_{xy}^2)/R^4 + O(1/R^6)$$

where σ_x^2, σ_y^2 and σ_{xy}^2 are the second moments of the energy distribution. The correlation term σ_{xy} cannot be obtained from the projections but the first term in the expression for m^2 gives the mass to better than 1%, so we can neglect the remaining terms. P_z is then obtained by the relation

$$P_z = (E^2 - m^2 - P_x^2 - P_y^2)^{\frac{1}{2}} .$$

The total four-vector for both sections is obtained by adding the four vectors from each section.

Much of our analysis is focussed on the distribution of the total momentum vector within our calorimeter. We express the orientation of the total momentum vector in terms of the azimuthal angle around the beam line and the pseudorapidity along the beam direction. The azimuthal angle, $\phi = \tan^{-1}(\frac{x}{y})$, is zero at the center of the calorimeter. The (c.m.)pseudorapidity is $\eta = -\ell n(\tan(\frac{\Theta}{2})) - \eta_o$ where Θ is the laboratory polar angle and $\eta_o = \ell n(2E_o/m_p)^{\frac{1}{2}}$.

In our analysis, we also examine the distribution of energy in the vertical, x, measuring counters. An average energy profile of jets centered on the calorimeter can be obtained by histogramming the energy deposition as a function of the vertical angle relative to the jet axis. The width of this profile is a measure of the jet-like character of the events.

Unfolding the effects of the calorimeter is carried out by a computer model of the calorimeter, taking into account the measured effects of energy resolution, shower spreading, energy loss at the edges, and the finite segmentation of the calorimeter. The unfolding of the measured yields entails the Monte Carlo simulation of the observed spectra of particles. We can then compare the yield from an idealized perfect calorimeter having the same acceptance to the yield resulting from the model of the real calorimeter. The ratio of these two yields allows us to make a correction to the raw yield. This unfolding was well constrained by the measured spectra.

4. The Data

The yields of total transverse momentum deposited into the calorimeter, $d\sigma/dP_t^2$, are shown plotted as a function of x_t where $x_t = 2P_t/\sqrt{s}$ in Fig. 3.

$$\text{Yield} = \frac{d\sigma}{dP_t^2} = (\text{no. of events})/(\text{no. of incid. protons})/(\text{no. of target protons/area})/\Delta P_t^2$$

The yields fall exponentially with different slopes for the three incident beam energies. Assuming $\frac{d\sigma}{dP_t^2} = A\exp(-Bx_t)$, we find B = 21, 26, 31 for beam momentum of 100, 200, and 340 GeV/c respectively.

In Fig. 4 we show the yields unfolded for the calorimeter effects. The fits now give B = 23, 27, 32 for beam momentum of 100, 200, and 340 GeV/c respectively.

The energy scale has an absolute overall uncertainty of less than 3%.

We have studied the η, ϕ and energy profile distributions to test our data with models ranging from e^+e^- jets to phase space distributions. To this end we have made spectra of the ϕ, η and energy profile distributions as a function of P_t of the jets. The energy profile is closely related to the

"jettiness" of the events. It would have a narrow width for jets and be broad for isotropic particles. The ϕ and η distributions would show how well our acceptance contains the jets. Figures 5 to 7 show examples of these spectra for 340 GeV/c beam momentum and for the indicated P_t window. These spectra display similar characteristics for the other two beam energies. Also, there was very little systematic change in these spectra for higher P_t. The exception was that the width of the energy profile decreased systematically. σ_x became 7% more narrow at P_t = 5.5 GeV/c.

5. Modeling of the Event Structure.

To interpret these distributions we examine Monte Carlo distributions generated with:

(a) two e^+e^-- like jets only;

(b) an uncorrelated-particle model;

(c) phase space with exponentially-limited P_t model;

(d) the 4-jet model.

In the next section, we will describe our computer Monte Carlo models for the above four cases. The results of the models compared with our spectra are summarized below:

(a) The two-jet model disagrees with all the ϕ, η and energy profile spectra of our data.

(b) The uncorrelated particle model shows good agreement with the ϕ, η and energy profile spectra. The model, however, blatantly disagrees with the magnitude and slope of the observed yield.

(c) The longitudinal phase space model, with exponential P_t dependence, reproduces the observed spectra when the P_t slope is suitably adjusted.

(d) The 4-jet model shows good agreement with all spectra.

(a) The "two-jet" model. In this model we assumed that the pp collision

produced e^+e^- jets over a large angular range. We also assumed that any other debris produced in the pp collision was negligible in our region of acceptance. The Monte Carlo program was developed to reproduce faithfully the features of the e^+e^- jets described in Reference [5].

In Fig. 5 we compare the energy profile of the data with this model. The data has a width which is about 1.5 times larger than the width expected from the Monte Carlo result for pure e^+e^- jets. In Fig. 6, we show the ϕ distribution for the data compared with the model. The model shows a plateau region which would allow for a definition of a fiducial region within which we could extract an invariant cross section for jets. The data, however, is much more narrow and has no plateau region.

(b) The uncorrelated particle model. In this model, we have assumed that the individual particles in inelastic collisions are created independently of one another. In our Monte Carlo model, we have generated the particles with azimuthal symmetry using the measured inclusive cross sections [6].

While the average azimuthally symmetric event produces a rather broad energy profile, we found that the events which produced the higher P_t contribution into the calorimeter were events where the energy profile was similar to the measured spectral shape. However, the yields from the uncorrelated particle model are much smaller and have a steeper slope in P_t than the observed yield. In Fig. 4, we show the event yield for 340 GeV from the uncorrelated particle model and note that the contribution relative to our observed yield at $x_t = 0.2$ is $\sim$10% and drops rapidly to 3% at $x_t = 0.3$.

We conclude that the uncorrelated particle model using the absolute measured inclusive single particle cross sections cannot account for our

observed yields. The observed yields must involve some correlation between the particles.

(c) The phase space with exponentially limited P_t model. In this model, we generated jets along the beam-target axis. We used the same longitudinal P spectrum as for the e^+e^- jets but we generated a P_t distribution with the functional form of $dn/dP_t^2 = e^{-4P_t}$. This method of Monte Carlo generation produced a spectrum of particles that was almost flat in rapidity within the acceptance of the calorimeter. The resulting yield closely matched the observed P_t dependence of the yield for 340 GeV. Figures 5 to 7 show that the spectra for this model qualitatively fit the observed spectra. The quality of the fit was good for all P_t at 200 and 340 GeV. However, we found that the Monte Carlo η spectrum at 100 GeV was displaced from the observed spectrum by .06 in the backward direction.

(d) The 4-jet Model. The parton scattering approach of Feynman et al. [7] was used as a starting point for the model described here. In this model, high P_t hadron jets arise from hard scattering of quarks and gluons. The scattered partons fragment into hadron jets. The remnant partons in the beam and target also fragment into hadrons to produce hadronic debris which would have limited P_t relative to the axis of the target and projectile. In our model, we have fragmented the scattered partons with the parameters fixed by those measured in e^+e^- collisions [5,8]. We have generated the debris by treating the remains of the collision as forward and backward jets. In summary, the model we have used here is:

$$p + P \rightarrow (\text{toward jet}) + (\text{away jet}) + (\text{beam jet}) + (\text{target jet})$$

where we have allowed all the jets to fragment independently of one another.

We fixed the P_t spectra of the scattered partons by matching the observed P_t

spectra. We have assumed that the angular spectra of the scattered partons is like the angular spectra of high P_t single particles.

Some Results of the 4-Jet model.

The 4-jet model predicts that upward fluctuations of the debris P_t contribute very strongly to the detected high P_t signal of the calorimeter. For example, the average P_t from debris for an event unselected for high P_t is only 0.6 GeV/c. However, for an event with a total of 5 GeV/c of P_t in the calorimeter, the debris contributes an average value of 1.6 GeV/c. Figure 8 shows the x_t spectra of the toward jet for events where the calorimeter detects an x_t of .5 to .6, and for events where the observed x_t is from .3 to .4. This result shows that the average debris contribution to the P_t will strongly increase the yield of events at high P_t. This figure also shows that the fractional contribution of P_t from the debris decreases at higher P_t.

The 4-jet model also predicts that the distortion of the jet axis found by summing the observed momentum 4 vectors incident on the calorimeter leads to a systematic shift of the jet axis toward the center of the calorimeter. This shift of the jet axis makes the measurement of the energy distribution around the jet axis more dispersed so that the jets appear to be less jet-like.

In Figures 5 to 7 we show the fit for this model to the spectra at 340 GeV. The ϕ and η distributions agree with the model to a few percent, while the energy profile of the data is $\sim$10% wider than the model prediction at 340 GeV. The model also fits with the same accuracy the spectra at higher P_t, showing the observed slight monotonic decrease in the width of the energy profile. For 200 GeV, this model fit the energy profile and ϕ spectra but produced an η spectra which was displaced by about .06 in the backward direction.

6. Comparisons with Other Experiments.

In Table 1 we list the characteristics of comparable experiments with beam momentum, solid angle, ϕ acceptance, cross section or yield at $x_t = 0.3$, and B where

$$\text{Yield or } \frac{Ed^3\sigma}{dp^3} \propto \exp(-Bx_t)$$

For the 100 to 130 GeV data, the most noticeable difference among the experiments are the variations of the slopes of the cross sections (or yields). The Table shows that the experiments with the larger acceptances have smaller slopes and larger magnitudes[12]. This trend continues at the higher energies.

In this paper, we do not try to extract the jet cross section from the overall yield.* We have found that our data does not lead to a straightforward extraction of the cross section. For example, the azimuthal spectrum displayed no plateau region from which we could define a fiducial region to extract a "jet" cross section. We note that the inclusive "jet" azimuthal spectrum from E395[3] agrees with our measurement in the lack of a plateau region. Reference [9], with 4π acceptance, finds no jet-like structure in their P_t region (P_t>3 GeV). However, experiments at the ISR with higher $\sqrt{s}$ and very high P_t have reported finding jet structures which accompany the high P_t single particle triggers [10].

In this experiment, the center of the calorimeter acceptance has been adjusted so that the calorimeter is approximately centered at 90^o for all three incident beam energies. In Fig. 9, we show the $\sqrt{s}$ dependence of the yield at $x_t = 0.35$. The data of this experiment is consistent with a power dependence of $\sqrt{s}$, yield $\propto \sqrt{s}^{-n}$ where n is a function of x_t. At this x_t,

*A future publication will address the problem of extracting a true jet cross section from the total signal.

$n = 6.2 \pm [0.3]^{\dagger,\dagger\dagger}$.

This figure also shows the $\sqrt{s}$ dependence expected from the uncorrelated particle model which exhibits $n \tilde{>} 8$. This model predicts a yield that is too small and has a slope that is much steeper than our data. On the same graph, we show the $\sqrt{s}$ dependence of the single particle pion cross section at the same x_t [11]. For $\sqrt{s}<30$ GeV, $n \simeq 8$, but for $\sqrt{s}>50$, n varies from 5 to 6. The $\sqrt{s}$ dependence of the yield in this experiment is similar to the $\sqrt{s}$ dependence of the pion cross section at $\sqrt{s}>50$ GeV. The naive point scattering model predicts $n = 4$. In summary, the $\sqrt{s}$ dependence of the yield is significantly different from that predicted by the uncorrelated particle model as well as that observed in single particle cross sections near the same $\sqrt{s}$.

7. Conclusions

We have measured high yields of events with large collective P_t in a 2.3 steradian calorimeter. The spectra of these events cannot be explained by events arising only from a jet (as observed in e^+e^- collisions), nor from fluctuations of the ordinary low P_t collisions. However, we cannot rule out the possibility that the observed events are produced in an azimuthally symmetric way with unexpectedly high P_t per particle. We find that the spectra of these events are approximately reproduced with a four-jet model, two e^+e^--like jets accompanied by debris from the remains of the projectile and the target protons.

Invariant cross sections could not be extracted from the yields because the data did not show acceptance independent qualities. The yields were found to vary as $\sqrt{s}^n$ at a fixed x_t. However, n is not independent of x_t because the exponential slopes of the yields systematically changed with $\sqrt{s}$. For $x_t=0.35$, $n \simeq 6.3 \pm [0.3]$.

†While the $\sqrt{s}$ dependence of the invariant cross section for jets has a definite theoretical interpretation, the $\sqrt{s}$ dependence of the yield may have a meaning only as some combination of the $\sqrt{s}$ dependence of the jet yield & the debris yield.

††The quoted error includes the estimated error of the procedure for unfolding the calorimeter effects.

The help of M. Delay, M. J. Fox, R. Krull, P. McManus, J. Rutherfoord, R. Sjoberg, and K. Turner is gratefully acknowledged. We thank the Fermilab staff for their assistance. This work was supported in part by the National Science Foundation and the U.S. Department of Energy.

References

[1] S. D. Ellis and M. B. Kislinger, Phys. Rev. D 9(1974); R. D. Field and R. P. Feynman, Phys. Rev. D 15(1976) 2590. For a review, and other references, see M. Jacob and P. V. Landshoff, Physics Reports 48(1978) 285.

[2] C. Bromberg et al., Phys. Rev. Lett. 43(1979) 565; C. Bromberg et al., Nucl. Phys. B134(1978) 189; C. Bromberg et al., Phys. Rev. Lett. 45(1980) 769.

[3] W. Selove, Proc. 19th Int. Conf. High Energy Physics, Tokyo (1978); W. Selove, Proc. of the 14th Rencontre de Moriond (Savoie, France, 1979) p. 401; and M. D. Corcoran et al., Phys. Rev. Lett. 44(1980) 514.

[4] P. M. Mantsch et al., Fermilab Report TM-721 (1978)(unpublished).

[5] G. Hanson, Proc. 13th Rencontre de Moriond (Savoie, France, 1978) Vol. II, p. 16.

[6] Alper et al., Nucl. Phys. B100(1975) 237; Singh et al., Nucl. Phys. B140 (1978) 189; D. Antreasyan et al., Phys. Rev. D 19(1979) 764, and references therein. Momentum-energy conservation in the Monte Carlo is approximate.

[7] R. P. Feynman et al., Phys. Rev. D18(1978) 3320.

[8] H. Schopper, TASSO data presented at the Goa Conference (Goa, India, 1979).

[9] M. Deutschmann et al., Nucl. Phys. B155 (1979) 307.

[10] A. L. S. Angelis et al., Phys. Scripta 19(1979) 116; M. G. Albrow et al., Nucl. Phys. B160(1979) 1; A. G. Clark et al., Nucl Phys. B160(1979) 397.

[11] The single pion cross sections at high P_t have been reported for $\sqrt{s}<30$ GeV by D. Antreasyan et al., Phys. Rev. Lett. 38(1977) 112; and for $\sqrt{s}>30$ GeV by A. L. S. Angelis et al., Phys. Lett. 79B (1978) 505.

[12] K. Pretzl, 20th International Conf. on High Energy Physics, Wisconsin (1980) unpublished. The NA5 collaboration reported measurements of high $\Sigma|P_t|$ events in a segmented calorimeter with $\lesssim 2\pi$ azimuthal acceptance. They reported a trend which linked larger magnitudes and smaller slopes for the cross section with larger azimuthal acceptance.

TABLE 1

$$\text{Yield or } E\frac{d^3\sigma}{dp^3} \sim \text{Exp}(-Bx_T)$$

Experiment	Trigger	Initial State	Trigger $\Delta\Omega$ (ster.)	Trigger $\Delta\phi$ (rad.)	$E\frac{d^3\sigma}{dp^3}$ (cm^2/GeV^2) or Yield (cm^2/GeV^2) at $x_t = .3$	B
This exp.	calori-meter	100 Gev pp	$\sim 2\frac{1}{2}$	$\sim 110^\circ$	$Y=1.3\times10^{-28}$	23
		200 Gev pp	$\sim 2\frac{1}{2}$	~ 110	$Y=1.3\times10^{-29}$	27
		340 Gev pp	$\sim 2\frac{1}{2}$	~ 110	$Y=4.4\times10^{-30}$	32
Ref. [9]	Bubble Chamber	110 Gev k^-p	~ 6 charge only	$\sim 180^\circ$	$\sim 5\times10^{-28}$	~ 24
E395[3]	Calori-meter	130 Gev pp	2	83°	$\sim 4\times10^{-29}$	~ 33
		200 Gev pp	2	83	$\sim 1\times10^{-29}$	~ 35
		400 Gev pp	2	83	$\sim 2\times10^{-30}$	~ 40
E260[2]	Calori-meter	200 Gev pBe	~ 1	$\sim 84^\circ$	$\sim 1\times10^{-29}$	~ 30
		200 Gev pp	~ 1	~ 84	$\sim 5\times10^{-30}$ (extracted jet cross section)	~ 31

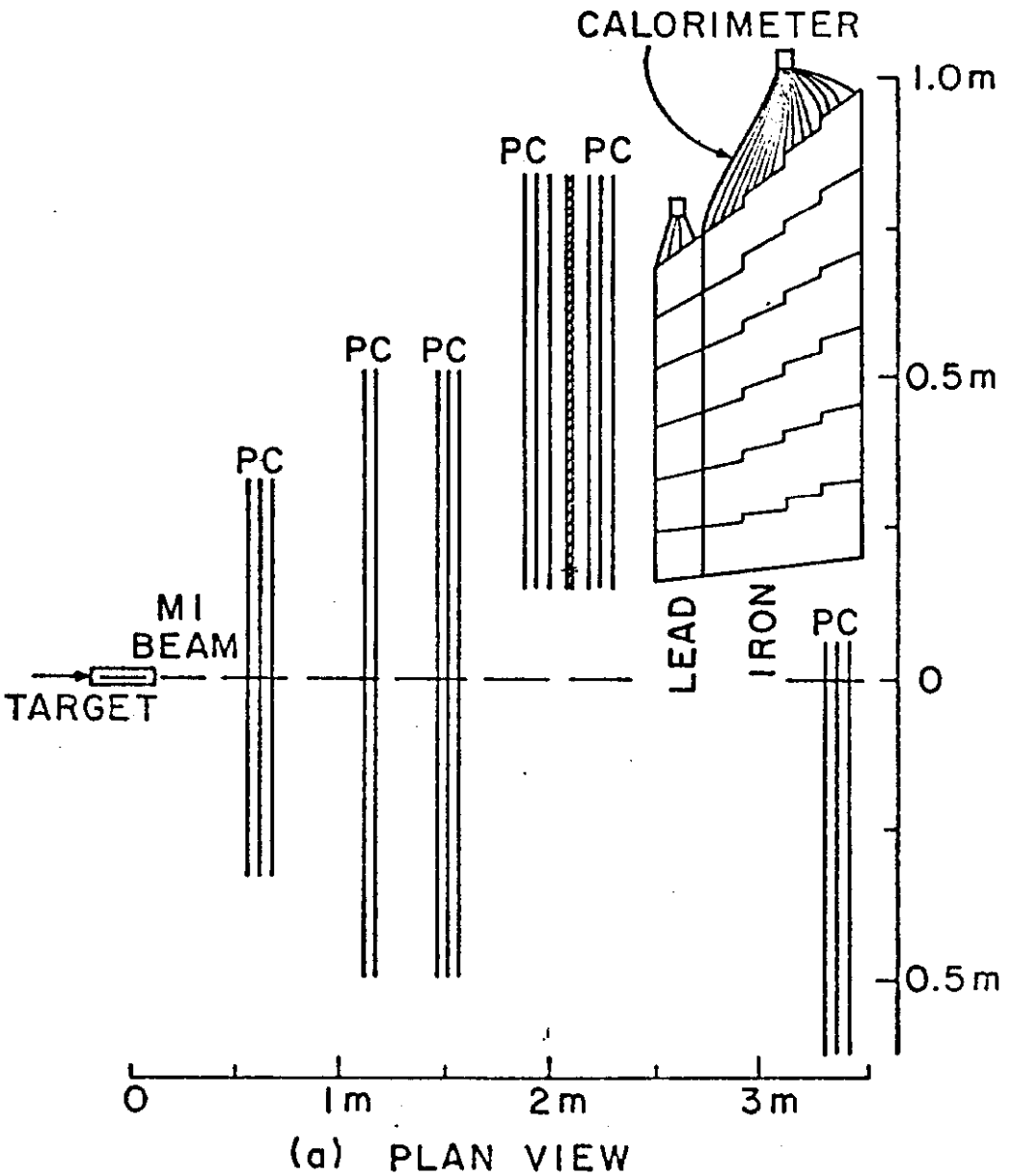

Fig. 1. Layout of the experiment. (a) plan view; (b) side view; (c) front view. The center-of-mass polar and azimuthal angles are shown on the calorimeter.

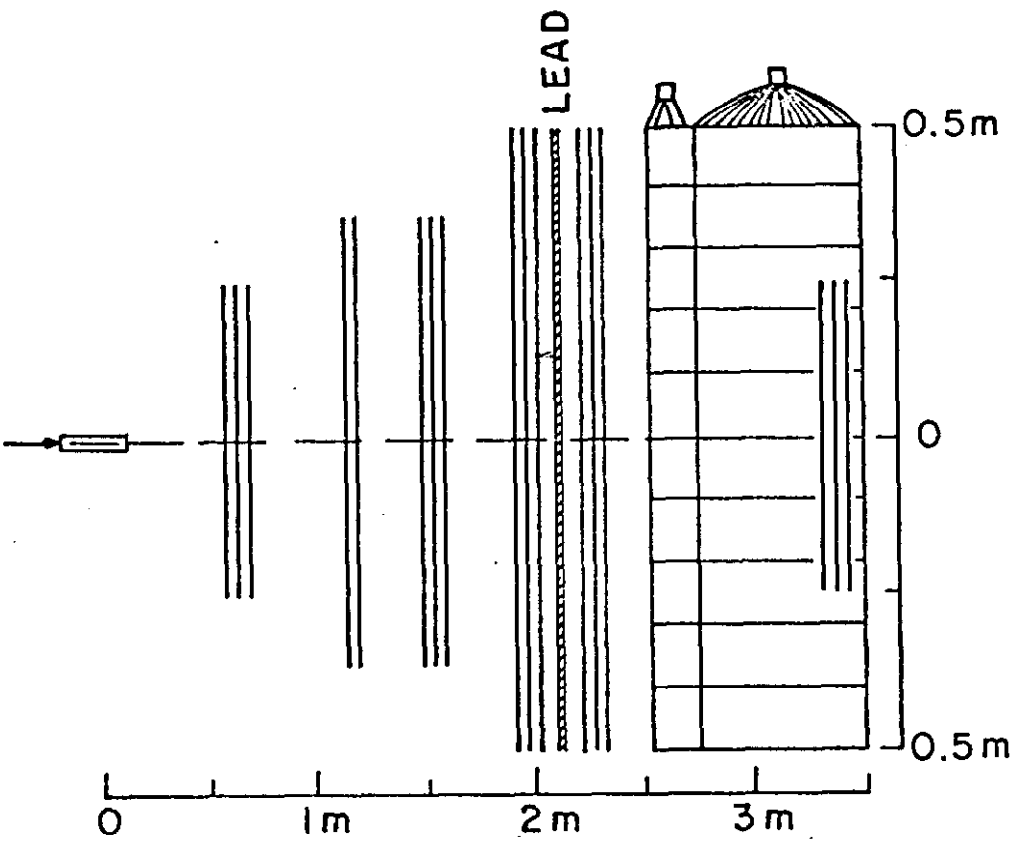

(b) ELEVATION

Fig. 1. Layout of the experiment. (a) plan view; (b) side view; (c) front view. The center-of-mass polar and azimuthal angles are shown on the calorimeter.

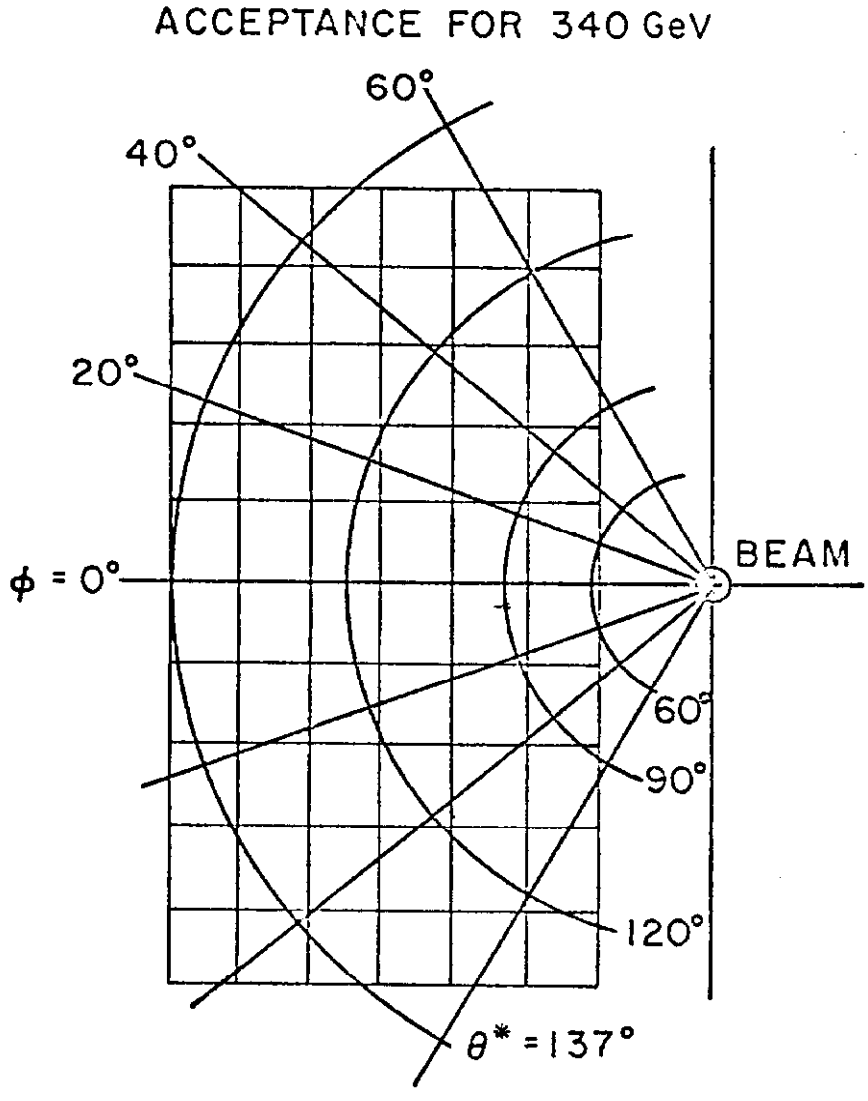

(c) FRONT VIEW OF CALORIMETER

Fig. 1. Layout of the experiment. (a) plan view; (b) side view; (c) front view. The center-of-mass polar and azimuthal angles are shown on the calorimeter.

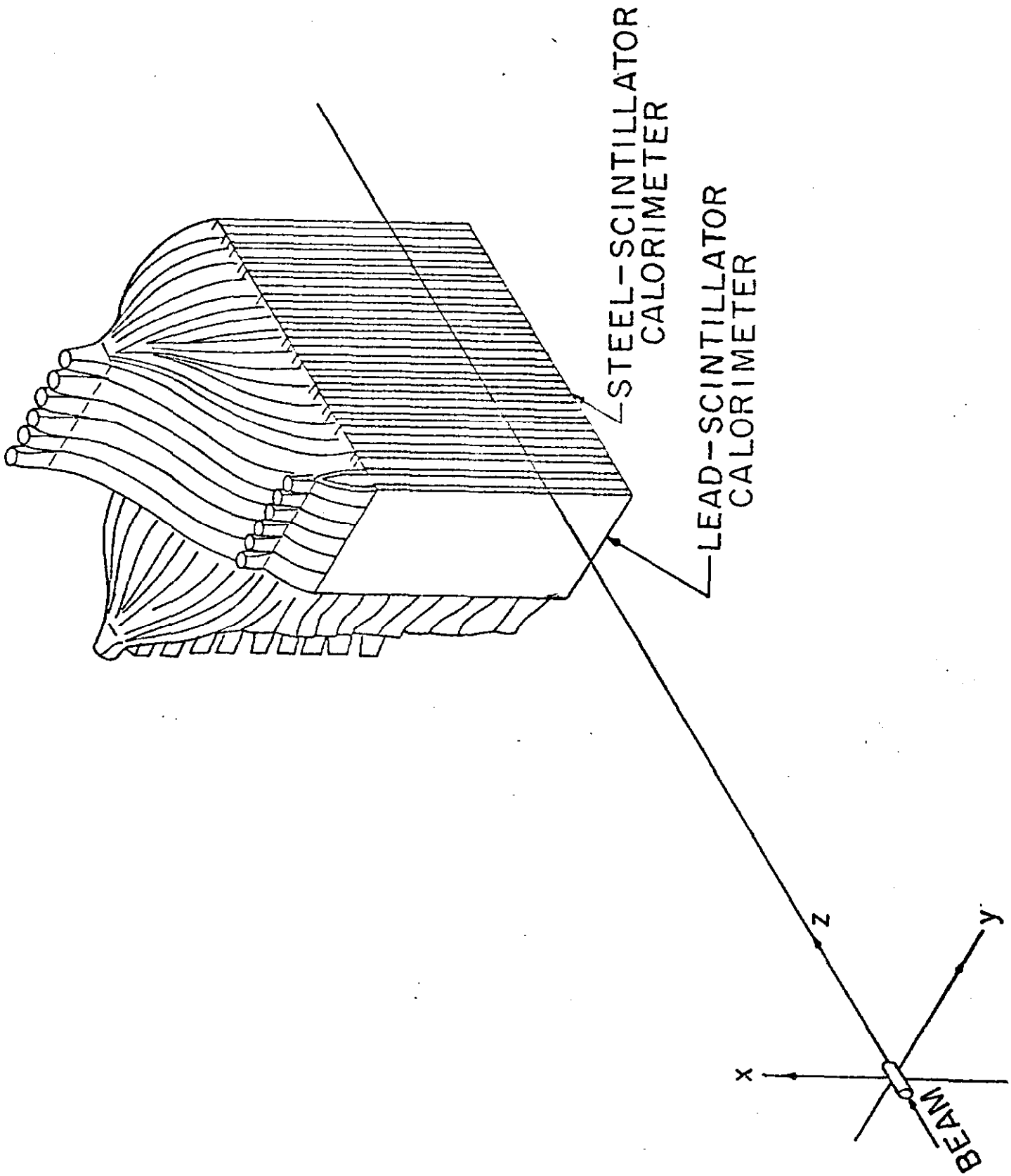

Fig. 2. Isometric view of the calorimeter.

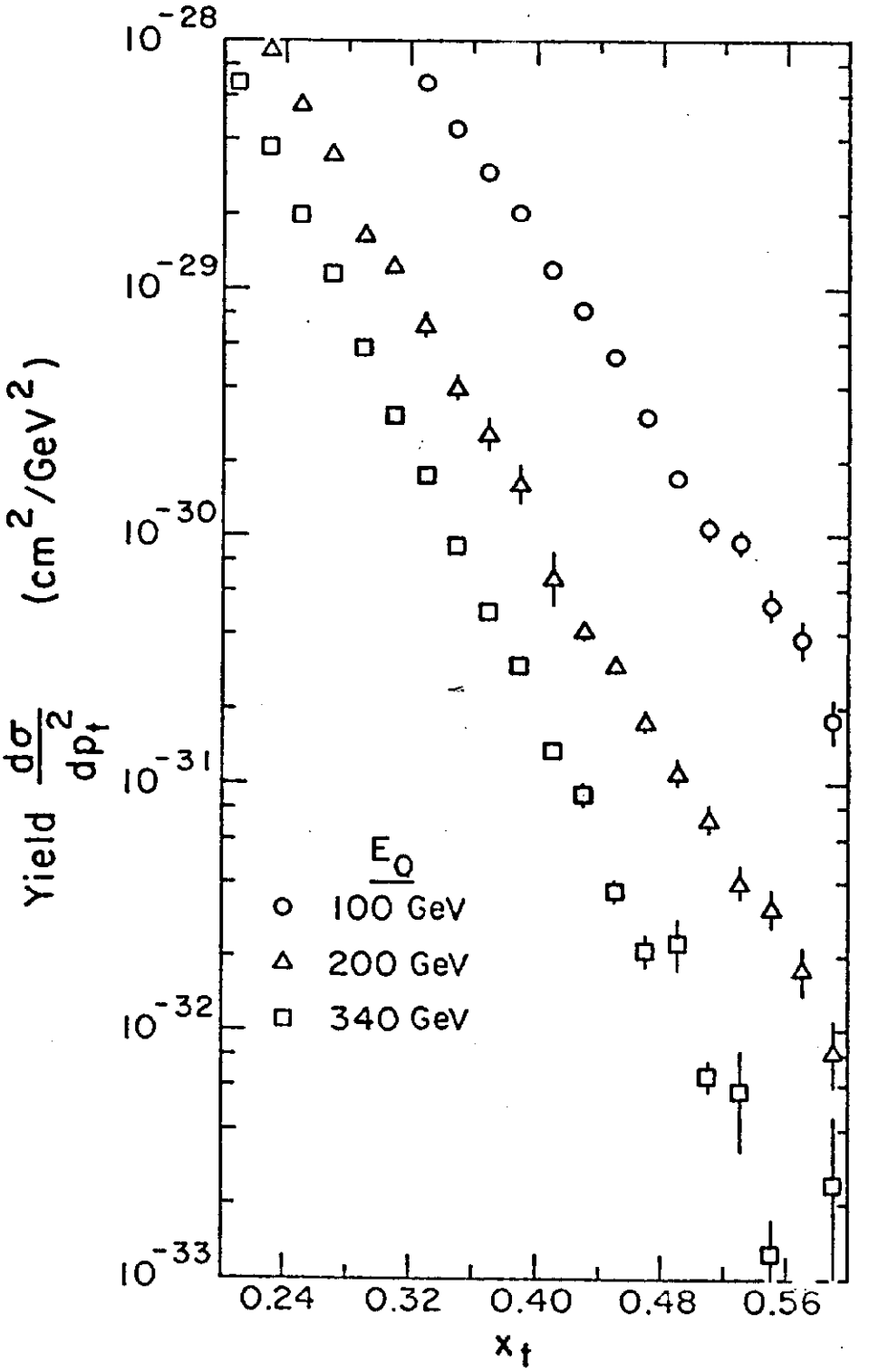

Fig. 3. Inclusive yield as a function of x_t at the 3 energies.

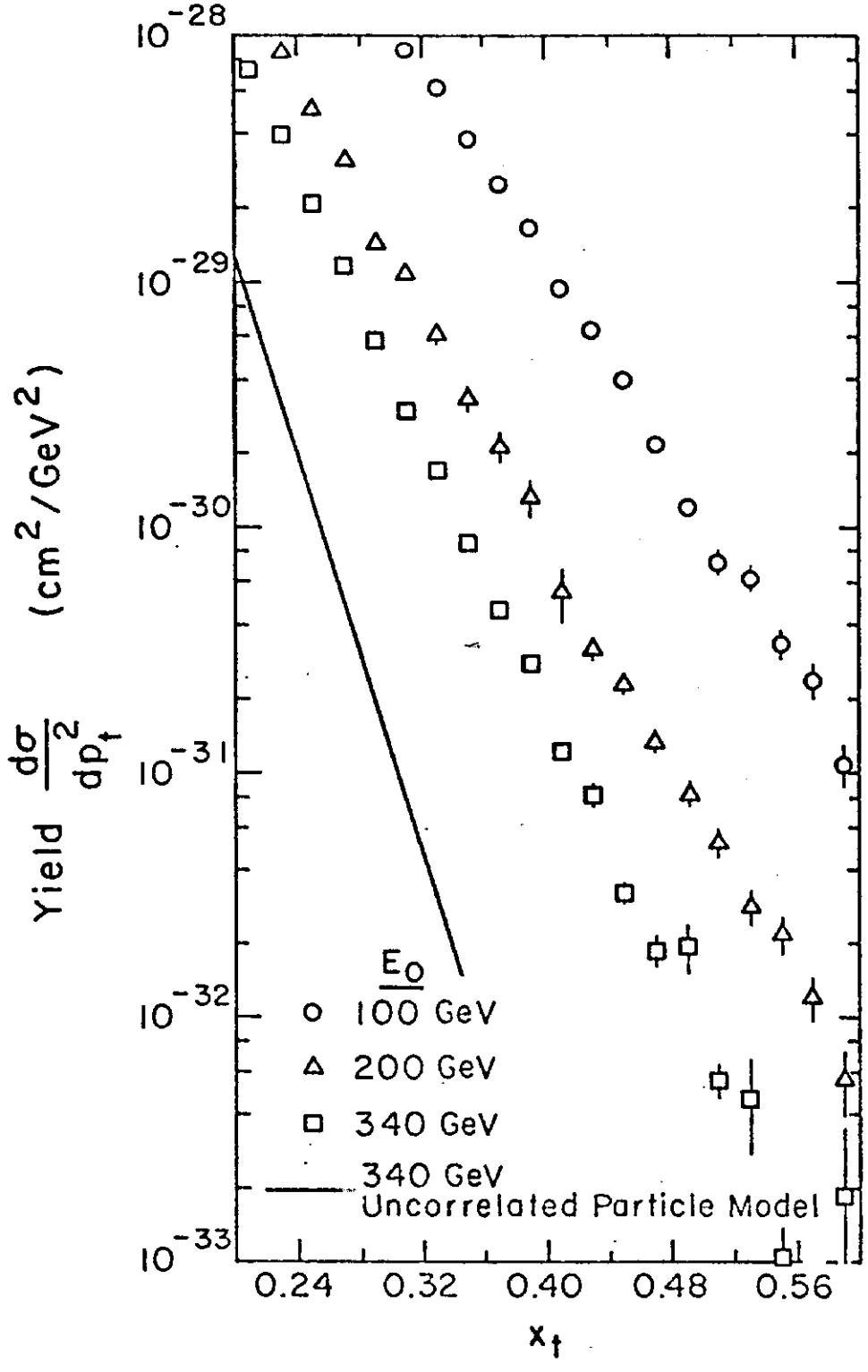

Fig. 4. Inclusive yield as a function of x_t unfolded for the calorimeter effects at the three energies.

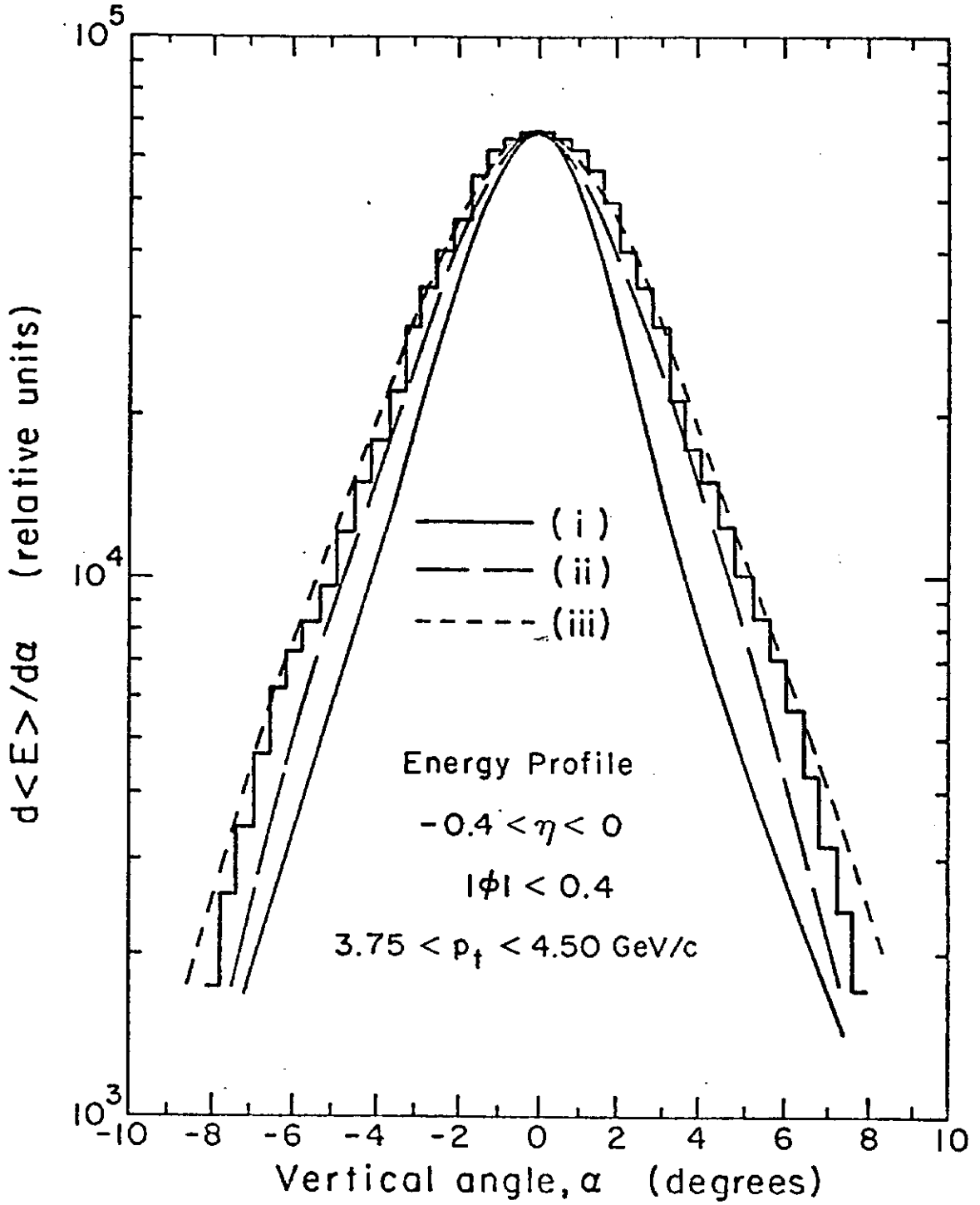

Fig. 5. Energy profile of the high P_t events as a function of the vertical angle. The histogram shows the data. The curves show the predictions from (i) e^+e^- jet only; (ii) 4-jet model; and (iii) phase space with exponentially limited P_t.

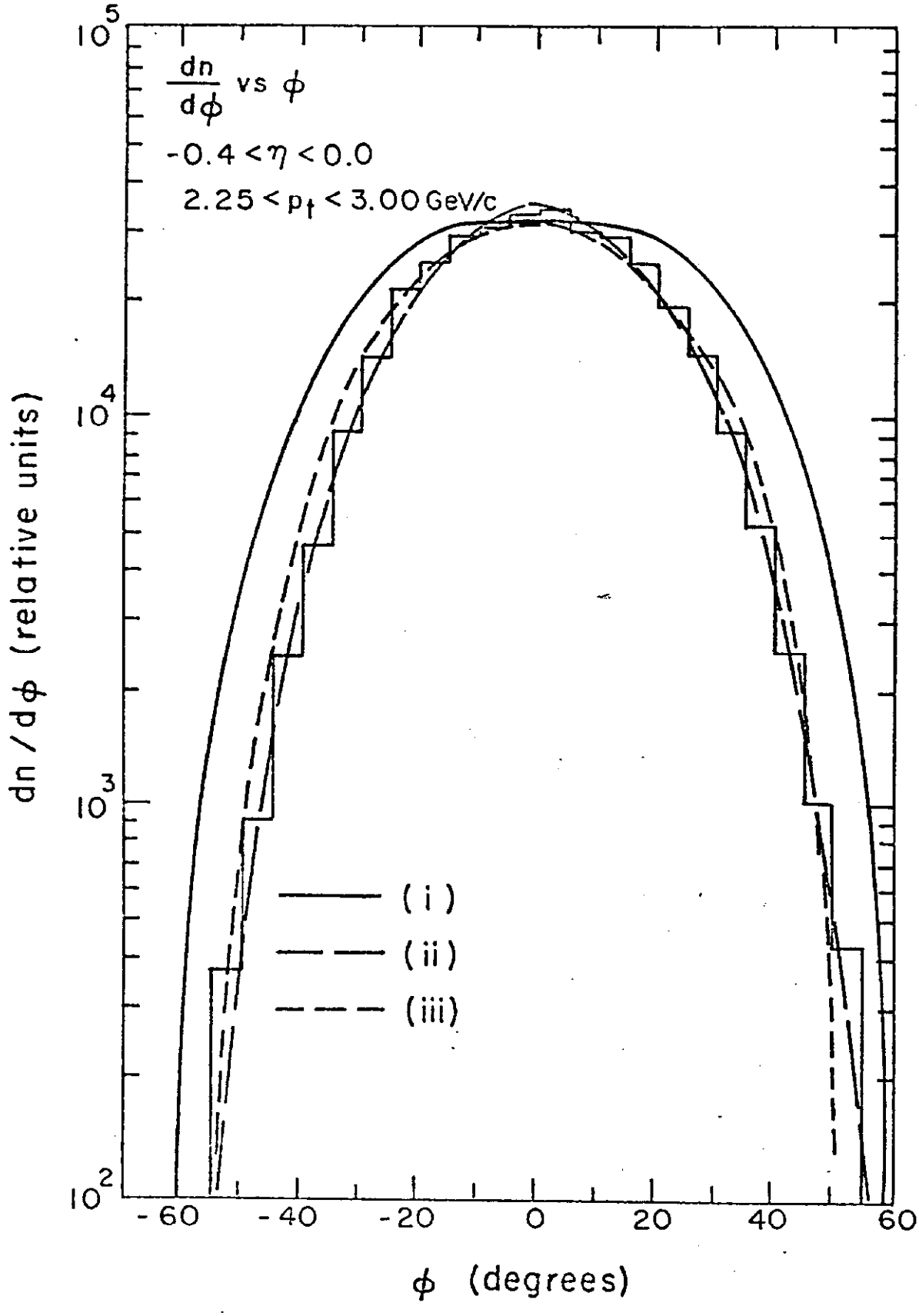

Fig. 6. The azimuthal distribution of the jet axes. The histogram shows the predictions from (i) e^+e^- jet only; (ii) 4-jet model; and (iii) phase space with exponentially limited P

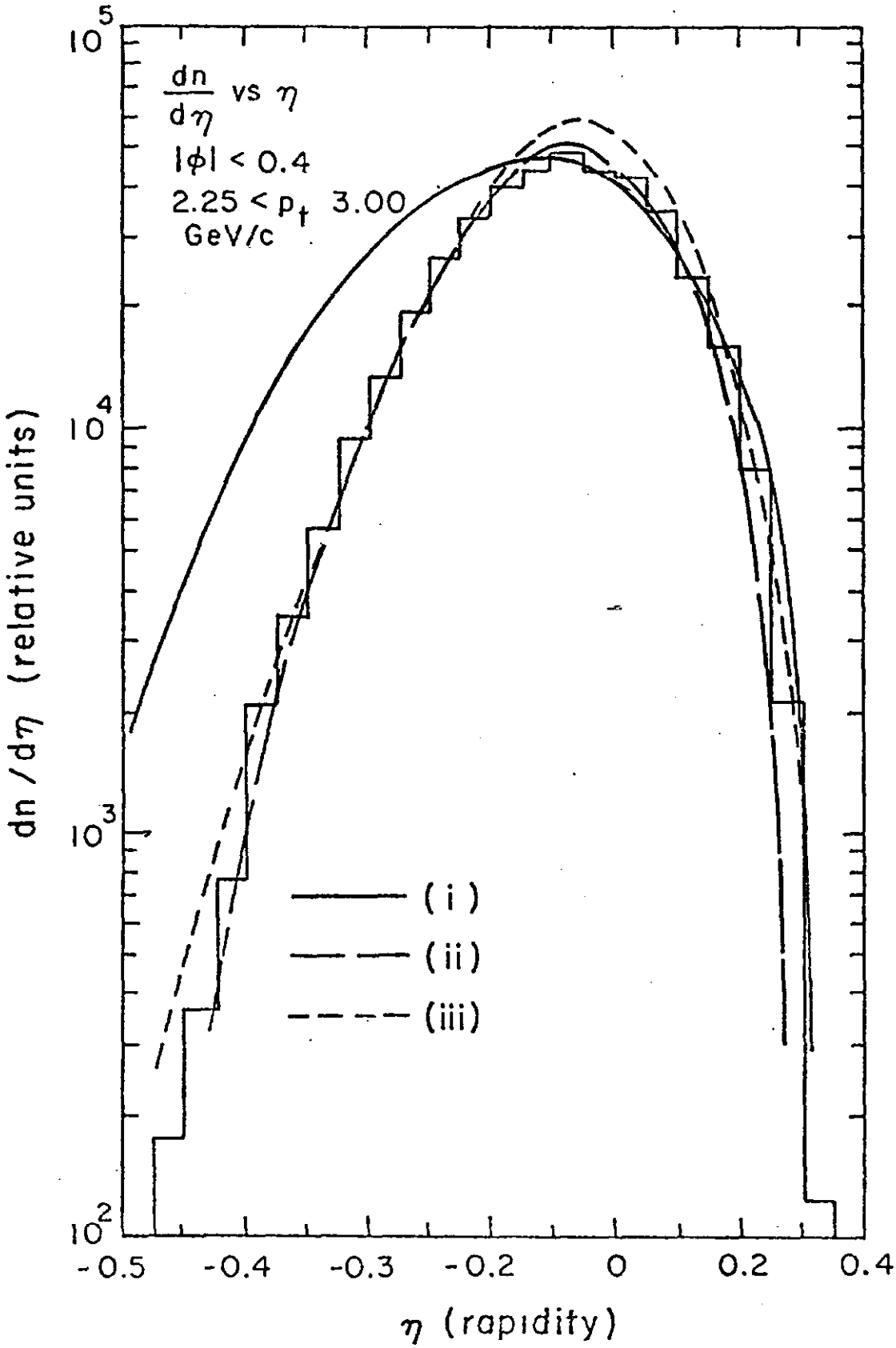

Fig. 7. The rapidity distribution of the jet axes. The histogram shows the predictions from (i) e^+e^- jet only; (ii) 4-jet model; and (iii) phase space with exponentially limited P .

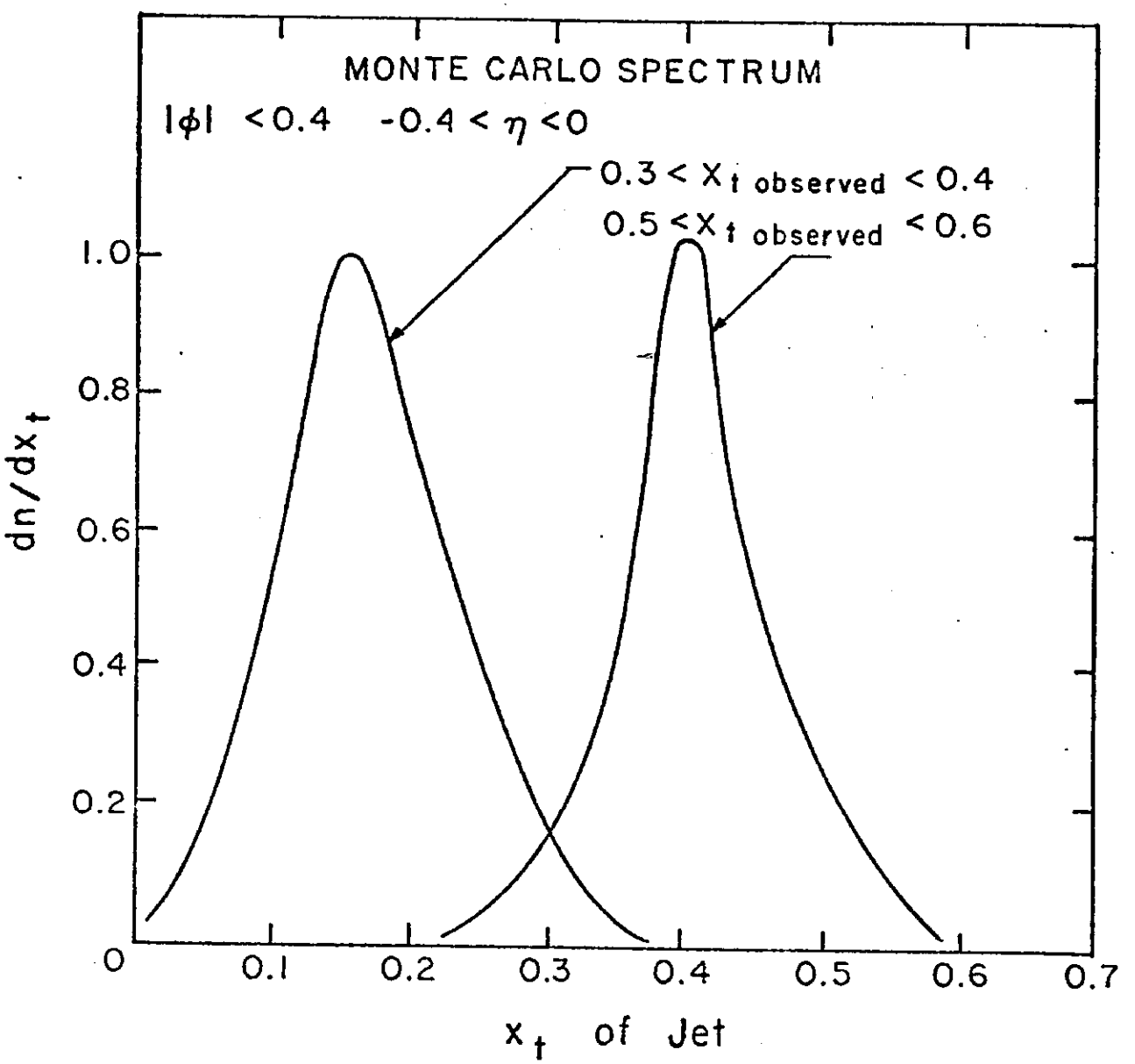

Fig. 8. The x_t spectra of the toward jets generated in a Monte Carlo program of events with fixed observed x_t.

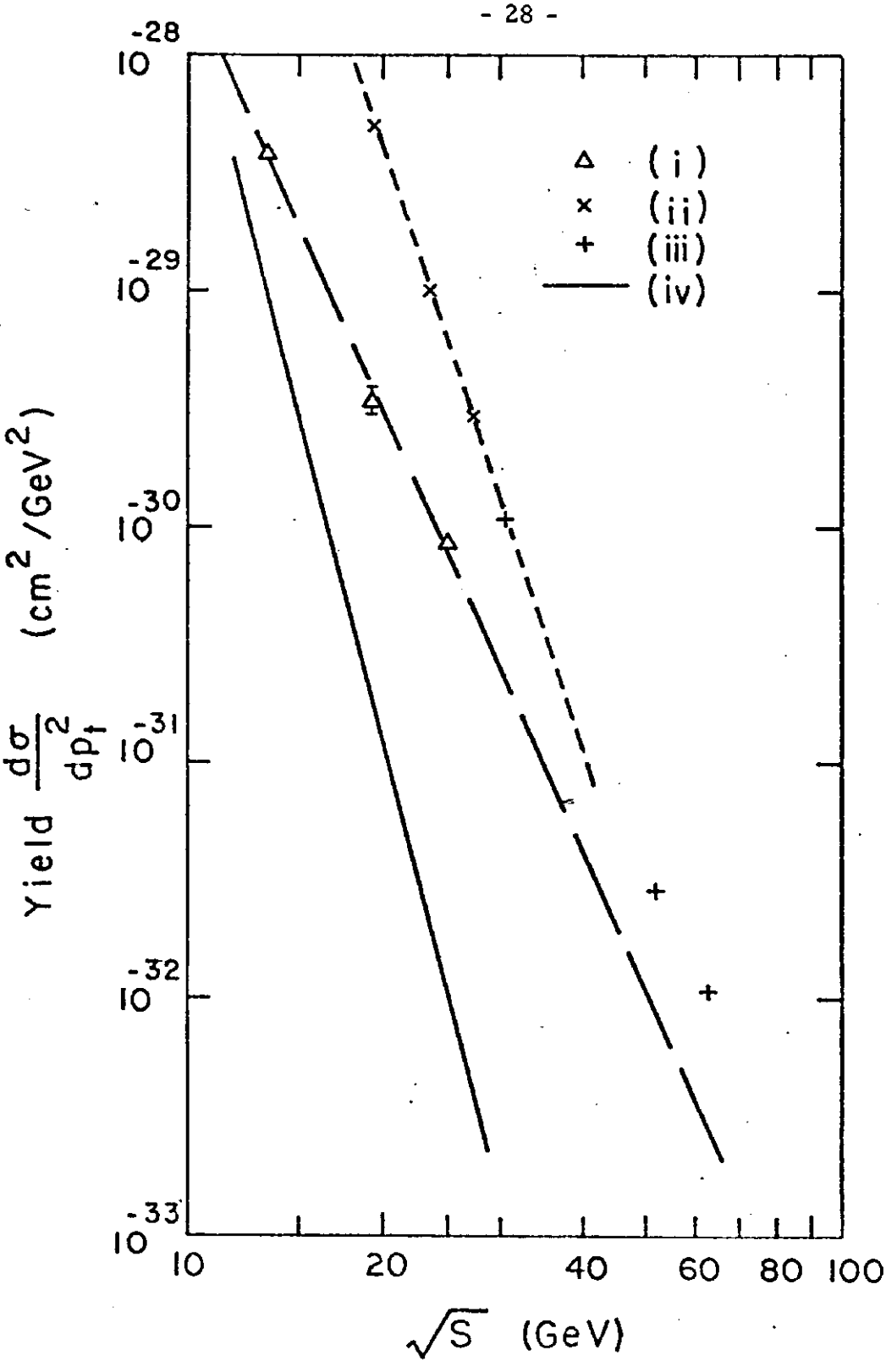

Fig. 9. The energy dependence of the yield at $x_t = 0.35$. Also shown is the prediction of the uncorrelated particle model. The single particle invariant cross section measurements are shown multiplied by 10^4: (i) This experiment; (ii) Chicago-Princeton $[\sigma(\pi^+)+\sigma(\pi^-)]/2 \times 10^4$; (iii) CCOR $\sigma(\pi^o) \times 10^4$; and (iv) uncorrelated particle model.